ELSEVIER

Tribology International 37 (2004) 783–789

TRIBOLOGY INTERNATIONAL

www.elsevier.com/locate/triboint

A study of mechanical shear bands in liquids at high pressure

Scott Bair [a,*], Clare McCabe [b]

[a] *Center for High Pressure Rheology, George W. Woodruff School of Mechanical Engineering, Georgia Institute of Technology, Atlanta, GA 30332-0405, USA*

[b] *Department of Chemical Engineering, Colorado School of Mines, Golden, CO 80401 USA*

Received 16 October 2003; received in revised form 29 April 2004; accepted 4 May 2004

Abstract

Shear localization has been observed in liquid lubricants flowing at high pressure. Two kinds have been identified: for stress-controlled plane Couette shear at high values of Nahme No., thermal runaway can result in the appearance of a band at mid-plane where the temperature and shear rate become localized. Alternatively, at high pressure and high shear stress, intermittent slip can be visualized along inclined bands for both planar Couette shear and squeeze film flows. These mechanical shear bands are responsible for the rate independent behavior that characterizes the traction transferred across the lubricant film in concentrated contact. We consider three models for shear band formation: Mohr–Coulomb slip, loss of ellipticity of Navier–Stokes equations, and non-monotonic stress–strain rate response. The observations that slip occurs for a ratio of shear to normal stress of about 0.1 and that bands form in two characteristic directions support both the Mohr–Coulomb failure criterion description and a change of character of the governing differential equations. Some evidence of constitutive instability is also presented; however, band orientation does not support this model.

Keywords: Shear bands; Localization; Limiting shear stress; High pressure; Molecular simulation; Normal stress difference

1. Introduction

The underlying mechanism of lubricated concentrated contact traction has been an outstanding tribological problem for at least 40 years. Concentrated contacts occur between non-conformal surfaces of machine elements made of high modulus solid materials. When relative motion occurs between such elements, a liquid lubricant is usually made available to separate the surfaces. The liquid must be piezoviscous in order to generate a usefully thick film in a process known as elastohydrodynamic lubrication. The traction transferred across the film results in mechanical energy loss in many components such as gears and bearings. Recently, interest in traction has been renewed due to advances in continuously variable gearless automotive transmissions. Here, high levels of traction are beneficial since the liquid film must replace the teeth of a conventional gear.

Historically, the study of concentrated contact traction has proceeded in two directions. The first approach has been to utilize the contact as a rheometer, where the traction force and contact area, which can be measured, yield an average shear stress. The sliding velocity and film thickness may also be measured to obtain an apparent shear rate. A rheological model is assumed and the necessary property relations are calculated. The second approach has been to perform measurements outside of contact using various high-pressure instruments as rheometers. These devices have generally been pressure cells such as falling body viscometers and diamond anvils cells, or impact devices. From these experiments, a model is formulated and calculations are checked against traction measurements.

Ideally, after 40 years, the two methods should have converged. Such is not the case. The necessity of extracting properties from averaged values has limited

* Corresponding author. Tel.: +1-404-894-3273; fax: +1-404-894-8336.

E-mail address: scott.bair@me.gatech.edu (S. Bair).

0301-679X/$ - see front matter © 2004 Elsevier Ltd. All rights reserved.
doi:10.1016/j.triboint.2004.05.002

contact based measurements to unrealistic assumptions. However, there is one aspect of traction for which there is agreement among techniques, namely, that there is a limit to the shear stress which may be sustained by a liquid film aside from the thermal softening limit. When this limit, the limiting shear stress, is attained, the shear stress becomes independent of rate. The limiting shear stress, τ_L, increases with pressure in approximate proportion to pressure, p, so that for high pressure,

$$\tau_L \approx \lambda p \tag{1}$$

where λ is the limiting traction (friction) coefficient. The fact that a viscous liquid film can respond to shear like a solid Coulombic frictional interface has become accepted within tribology in spite of the obvious contradiction.

The idea that the shear stress borne by a liquid film may be limited by the stress at which the shear deformation becomes localized was first advanced by Plint [1]. The mechanism, proposed by Plint and others later, was that of a thermally softened region in the middle of the film where the temperature and shear rate were localized. However, the relationship between pressure and limiting stress was never clarified. In 1986, Evans and Johnson [2] proposed that mechanical shear bands as seen in solid polymers may be responsible for the observed limiting stress. For glassy polymers which deform by shear banding, the pressure dependence of the yield strength is well documented (see Ref. [3] and the references therein).

Before discussing mechanical shear bands, we should be aware that the thermal "adiabatic" shear band has been described analytically and observed experimentally in a liquid sheared under controlled stress and high pressure [4]. The combined effect of viscous heating and thermal sensitivity of a fluid can be represented by the Nahme–Griffith number, Na, which signifies the ratio of temperature rise due to viscous heating to the temperature rise necessary to make a significant (i.e. O(1)) change in the viscosity. The Nahme–Griffith number for simple steady shear is,

$$Na = \frac{\beta \tau^2 h^2}{\mu k} \tag{2}$$

where β is the temperature–viscosity coefficient, h is the gap between isothermal parallel plates and k is the liquid thermal conductivity. If we apply a shear stress, τ, and solve the coupled energy equation and equation of motion for a Newtonian liquid, we find that there is no steady solution for the distribution of shear rate, $\dot{\gamma}$, when $Na > 3.5138$ [4]. We can, of course, apply a shear stress which results in large values of Na. In this case, the solved temperature becomes unbounded at the midplane and a visible band appears in visualization experiments [4]. The implications of thermal shear bands in lubrication have not been explored.

We believe that the first observations of shear bands in liquids were obtained in the Center for High Pressure Rheology [5]. Mechanical shear bands have been visually observed by Bair et al. [6] and Ohno et al. [7] in planar Couette shear in liquids compressed to greater than the glass transition pressure and somewhat below the glass transition pressure [6]. In these studies, the pressure cells utilized by both laboratories are similar and are described in detail in Ref. [6].

A unique property of shear bands in liquids below the glass pressure is that the optical effect which causes them to be visible (probably a refractive index gradient) persists only for a time roughly equal to the shear relaxation time [8]. The mechanical shear bands rotate with the rotation of the continuum for only a small angle before disappearing. We should also point out that the bands are not birefringence fringes. The interference bands observed and reported with our flow cell between crossed polarizers result from molecular alignment and are quite different [8] from shear bands. Shear bands, of the mechanical kind in liquids, operate in two distinct directions. In simple shear, the first type makes a small angle with the flow direction and the second type is approximately perpendicular to the shearing surfaces. This is illustrated in Fig. 1 where the angles made with the surface by the first and second type of shear band are θ_1 and θ_2, respectively. For squeeze film flow, the shear bands are observed to criss-cross the film at nearly, but not exactly, 45° to the surfaces [9]. Mechanical bands as we observe them cannot slip continuously as they become pinned at the surfaces.

In this progress report, we seek an analytical framework with which to model mechanical shear band formation and to calculate the effects on the relationship between observable flow kinematics and measurable stresses.

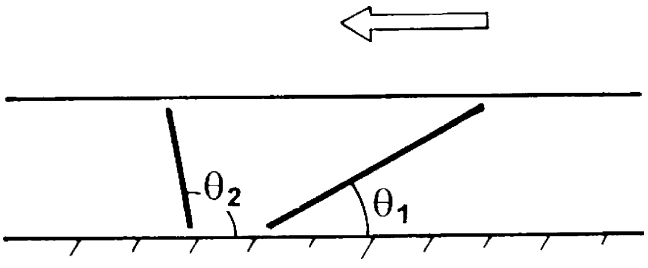

Fig. 1. Schematic illustrating shear band angles. The lower surface is stationary and the upper surface moves in the direction indicated by the arrow.

2. Models and supporting experiments

2.1. Mohr–Coulomb

The Mohr–Coulomb failure criterion has proven useful for predicting material failure or slip for glassy polymers [3], as well as soils. Failure occurs when the ratio of shear stress, τ, to compressive normal stress, $-\sigma$, on any plane reaches the value of the coefficient of internal friction, ϕ. This is illustrated in Fig. 2 where the cross-film coordinate is y and the motion is in the $-x$ direction. The pressure is defined as $p = -(\sigma_x + \sigma_y)/2$. We define for slip conditions, $\lambda = \tau/p$ and $\zeta = (1/2p)(\sigma_x - \sigma_y)$. The compressive normal stress on a plane at arbitrary rotation, θ, is,

$$-\sigma_\theta = p + \zeta p \cos 2\theta - \tau \sin 2\theta \tag{3}$$

The shear stress is

$$\tau_\theta = \tau \cos 2\theta + \zeta p \sin 2\theta \tag{4}$$

Slip occurs on a plane for which

$$\frac{|\tau_\theta|}{-\sigma_\theta} = \phi \tag{5}$$

and since there can be no greater value of $|\tau_\theta|/-\sigma_\theta$, we know that

$$\frac{\mathrm{d}}{\mathrm{d}\theta}\left(\frac{\tau_\theta}{-\sigma_\theta}\right) = 0 \tag{6}$$

on a shear band. Dividing (4) by (3) and differentiating, we find using (6) that

$$\lambda^2 + \zeta^2 - \lambda \sin 2\theta + \zeta \cos 2\theta = 0 \tag{7}$$

There are two solutions for θ in (7), θ_1 and θ_2. The coefficient of internal friction can then be found from

$$\phi = \frac{\lambda \cos 2\theta + \zeta \sin 2\theta}{1 + \zeta \cos 2\theta - \lambda \sin 2\theta} \tag{8}$$

using either value of shear band angle. Note that the first normal stress difference is $N_1 = 2p\zeta$.

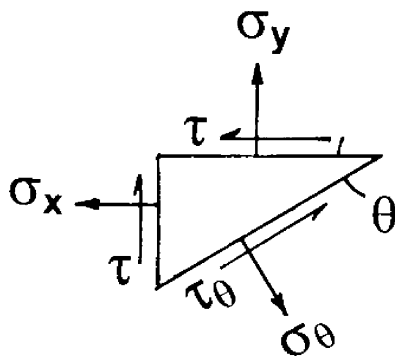

Fig. 2. Stresses on an element of liquid. See Fig. 1 for orientation.

Two micrographs of mechanical shear bands are shown in Fig. 3. The liquids studied were 5P4E, a 5-ring polyphenyl ether of molecular weight 450 and MCS1218, a cycloaliphatic hydrocarbon with molecular weight of 1000 g/mole, both of which are high traction liquids. The measured shear band angles are listed in Table 1 along with the parameters λ, ζ, ϕ, and N_1/τ obtained from Eqs. (7) and (8).

We have also generated flow curves for these high traction liquids using a pressurized Couette viscometer, which is described in Ref. [10]. Note that slightly lower pressures were utilized for the viscometer measurements. The results, shown in Fig. 4, are typical for liquids used as lubricants. A Newtonian regime is evident for $\tau < 5$ MPa. Shear-thinning occurs at higher shear stress, followed by a plateau of stress where the response is rate-independent at a limiting stress. We can compare the limiting stress (given by the horizontal solid line) with λp obtained from the shear band angles using the Mohr–Coulomb criterion (the dashed line). The agreement is satisfactory.

Measurements of normal stress difference have been made for one of the liquids, 5P4E [11]. A torsional flow measurement between rotating parallel plates was obtained in a pressure vessel, giving the difference between the first and second normal stress differences, N_1–N_2. Typically, $|N_2| \ll |N_1|$ so that for our purposes,

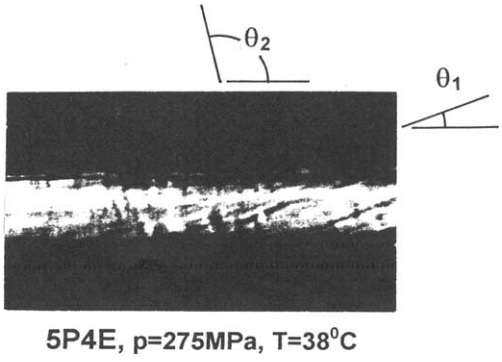

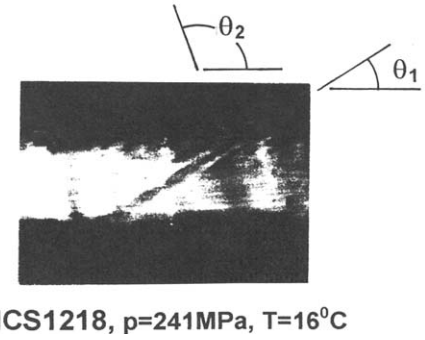

Fig. 3. Micrographs of mechanical shear bands observed at the given state conditions.

Table 1
Shear band angle measurements (see Fig. 3 for conditions)

Liquid	T (°C)	p (MPa)	θ_1 (°)	θ_2 (°)	λ	ζ	ϕ	N_1/τ
5P4E	38	275	18	102	0.091	0.0525	0.106	1.16
MCS1218	16	241	32	107	0.170	0.195	0.268	2.29

we can neglect N_2. Note that two data points for which viscous heating was excessive have been removed [11]. Also plotted is the theoretical value of $N_1 = 2\tau^2/NkT$ for the terminal regime, where N is the number of molecules per unit volume and k is the Boltzmann constant. The dashed line represents the result from shear band angle measurements, $N_1 = 2(\zeta/\lambda)\tau$. From Fig. 5, it is not unreasonable that N_1 would reach the dashed line required by Mohr–Coulomb for shear stress of 10–30 MPa. We use molecular simulations on another liquid to support this possibility.

Non-equilibrium molecular dynamics (NEMD) simulations have recently shown remarkable agreement with rheological measurements at high pressure and high shear stress for the shear viscosity of squalane, a highly branched isomer of C_{30} [12]. By recognizing that applying the standard rheological analysis technique of temperature–time superposition, we were able to bring very high-pressure viscosity experiments and simulation into comparable regions of the reduced viscosity–strain rate curve, allowing comparison between experiment and the NEMD and providing the first experimental verification of the NEMD simulation in the non-Newtonian regime. Similar high-pressure NEMD simulations have also been performed for trioctylmethane. In this work using a united atom model [13,14] for the hydrocarbon, a series of simulations were performed at 372 K and pressures in the gigapascal range to determine the strain rate dependant viscosity [15]. At these high pressures, and hence density, the relaxation time of the system, is very long and so the non-Newtonian region extends to low (for NEMD) shear rates ($<10^8$ s^{-1}) on the scale accessible by simulation. Hence, reaching the Newtonian plateau requires very lengthy simulations. From the calculation of the pressure tensor during the simulations using the usual Irving Kirkwood expression [16], we can extract the first normal stress difference, N_1. Fig. 6 shows the first normal stress difference for trioctylmethane, obtained by the NEMD simulation to very large shear stress. It is clear from the figure that for τ greater than about 30 MPa, N_1 can reasonably be described as a constant multiple of τ of between 1 and 2. This result gives credibility to the values of N_1/τ obtained from the micrographs and listed in Table 1. We should note that the simulation results of Fig. 6 were obtained without previous knowledge of the N_1/τ ratio obtained from shear bands and as such represent true predictions.

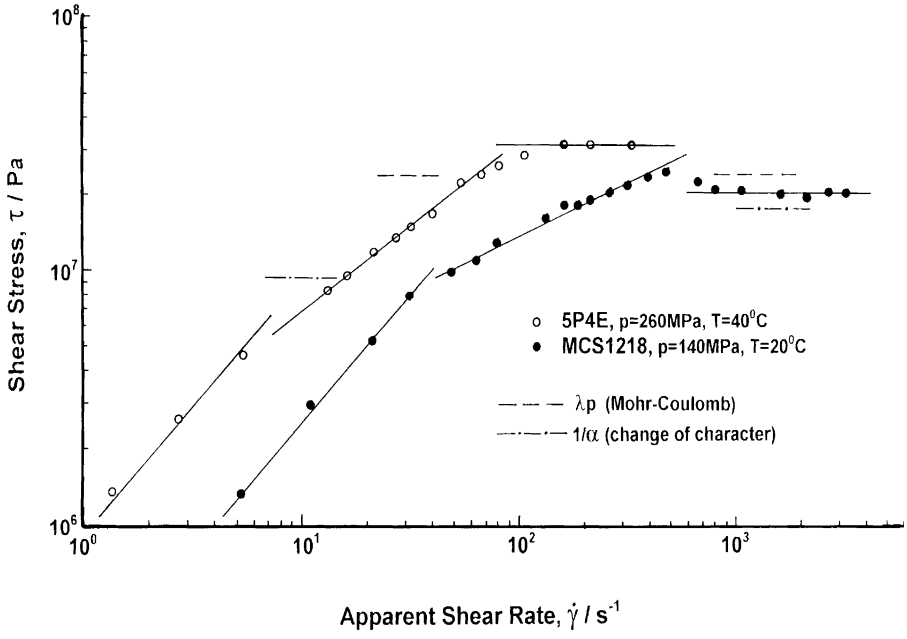

Fig. 4. Flow curves for the liquids of Fig. 2. Broken lines are λp obtained from shear band angles.

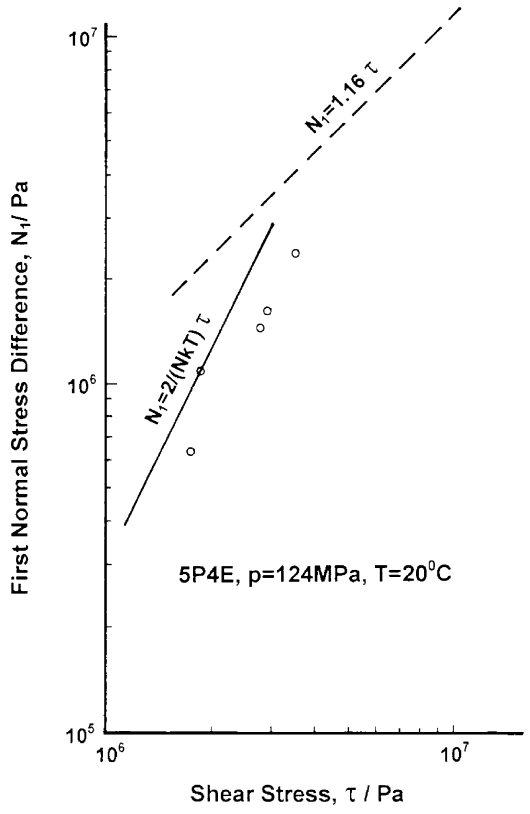

Fig. 5. Normal stress difference by rheometry for one of the liquids shown in Figs. 3 and 4 from [11].

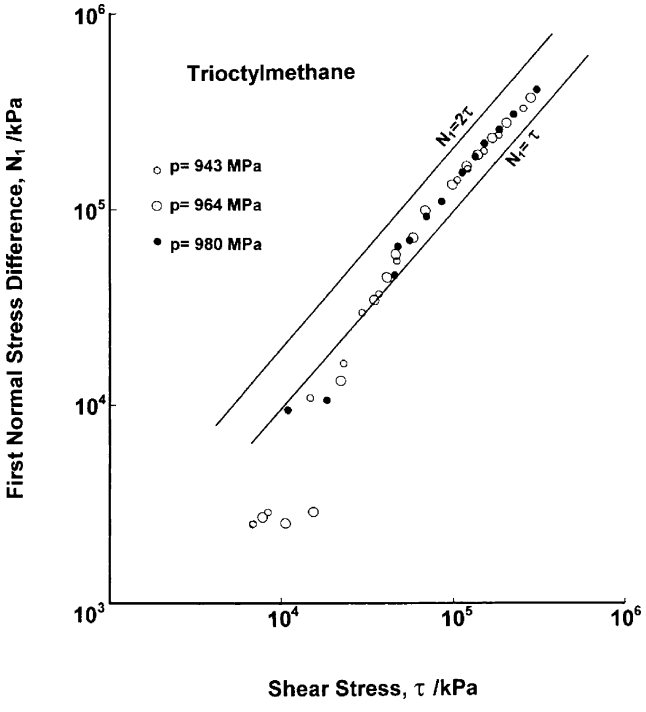

Fig. 6. Normal stress difference by molecular simulation for a low molecular weight hydrocarbon.

2.2. Change of character of Navier–Stokes equations

Of the models that we have examined to date, the Mohr–Coulomb theory is most consistent with experiment. However, the microscopic or physical origin of the coefficient of internal friction has not been discovered. Renardy [17] found that the introduction of piezoviscosity into the incompressible Navier–Stokes equation brings about the possibility of change of character. This loss of ellipticity of the equations of motion has been associated with shear bands in solids and discontinuities in compressible flow.

Consider the two-dimensional creeping flow of an incompressible liquid. The continuity equation is

$$u_x + v_y = 0 \tag{9}$$

where u and v are velocities in the x and y directions, respectively, and the subscripts on velocities represent partial differentiation. The Navier–Stokes equations reduce to:

$$\frac{\partial p}{\partial x} = 2\frac{\partial}{\partial x}(\mu u_x) + \frac{\partial}{\partial y}[\mu(v_x + u_y)] \tag{10}$$

$$\frac{\partial p}{\partial y} = 2\frac{\partial}{\partial y}(\mu v_y) + \frac{\partial}{\partial x}[\mu(v_x + u_y)] \tag{11}$$

It may seem a contradiction to consider an incompressible piezoviscous liquid since the changes in viscosity, μ, with pressure arise from compression of the free volume. However, at high pressures where the free volume fraction is very small, a 1% reduction in volume results in one or two orders of magnitude increase in the viscosity. As pressure increases, the liquid becomes both less compressible and more piezoviscous. Then, in much the same spirit that linear elastic mechanics can be useful within the plastically deforming zone of a crack tip, we will consider incompressible piezoviscosity. The local pressure–viscosity coefficient is

$$\alpha = \frac{1}{\mu}\frac{\mathrm{d}\mu}{\mathrm{d}p} \tag{12}$$

and the viscosity gradients become,

$$\frac{\partial \mu}{\partial x} = \alpha\mu\frac{\partial p}{\partial x} \text{ and } \frac{\partial \mu}{\partial y} = \alpha\mu\frac{\partial p}{\partial y} \tag{13}$$

Substitution of (13) into (10) and (11) gives,

$$(2\mu\alpha u_x - 1)\frac{\partial p}{\partial x} + \mu\alpha(u_y + v_x)\frac{\partial p}{\partial y} + \mu(u_{xx} + u_{yy}) = 0 \tag{14}$$

$$(2\mu\alpha v_y - 1)\frac{\partial p}{\partial y} + \mu\alpha(u_y + v_x)\frac{\partial p}{\partial x} + \mu(v_{xx} + v_{yy}) = 0 \tag{15}$$

These are the Navier–Stokes equations for an incompressible piezoviscous liquid. Let $a_1 = \alpha(u_y + v_x)$, $a_2 = 2\alpha u_y - 1/\mu$, $a_3 = 2\alpha v_y - 1/\mu$. Then (14) and (15)

become,

$$a_2\frac{\partial p}{\partial x}+a_1\frac{\partial p}{\partial y}+u_{xx}+u_{yy}=0 \tag{16}$$

$$a_1\frac{\partial p}{\partial x}+a_3\frac{\partial p}{\partial y}+v_{yy}+v_{xx}=0 \tag{17}$$

Differentiating (9), we obtain

$$u_{xx}+v_{yx}=0 \tag{18}$$

$$u_{xy}+v_{yy}=0 \tag{19}$$

The set of partial differential Eqs. ((16)–(19)) has the characteristic equation

$$\left[1+\left(\frac{\mathrm{d}y}{\mathrm{d}x}\right)^2\right]\left[\alpha_2\left(\frac{\mathrm{d}y}{\mathrm{d}x}\right)^2-2a_1\left(\frac{\mathrm{d}y}{\mathrm{d}x}\right)+a_3\right]=0 \tag{20}$$

and the characteristics have slopes of

$$\frac{\mathrm{d}y}{\mathrm{d}x}=\pm i,\qquad \frac{a_1\pm\sqrt{a_1^2-a_2a_3}}{a_2} \tag{21}$$

Obviously, two characteristics are always imaginary but two may or may not be real. The foregoing derivation may be found in more detail in Ref. [18] where it is postulated that both secondary flows and unbounded pressure gradients are possible at the change of character. Subsequent numerical studies have shown that the pressure gradients remain finite but secondary flows do develop. If we expand the expression within the radical in (21), we find that no characteristics of the equations of motion are real (i.e. the set of equations of motion is elliptical) only for

$$\mu\sqrt{(u_y+v_x)^2-4u_xv_y}<1/\alpha \tag{22}$$

Since the LHS of Eq. (22) is the maximum principal shear stress, τ_1, the equations of motion change character when the maximum principal shear stress attains the value of the reciprocal of the pressure–viscosity coefficient. For $\tau_1>1/\alpha$, there are two real characteristics which represent the directions, $\mathrm{d}y/\mathrm{d}x$, along which discontinuities in the velocity may propagate.

We have measured the viscosities of both 5P4E and MCS 1218 using a pressurized falling body viscometer. From the measurements, the pressure–viscosity coefficient, α, was determined. For 5P4E, $\alpha=0.105$ MPa^{-1} and for MCS1218, $\alpha=0.056$ MPa^{-1} for the respective temperature and pressure shown in Fig. 4. The shear stress for change of character, $1/\alpha$, is plotted in Fig. 4 as the dot-dashed line. For both liquids, the character of the incompressible piezoviscous Navier–Stokes equations is no longer elliptical at the level of shear stress for which rate independence is observed. We believe this may provide an explanation for the two types of shear bands and their nucleation and propagation.

2.3. Non-Monotonic shear stress

Some important constitutive laws predict that the shear stress will first increase with shear rate followed by a decrease with rate after reaching a local maximum. Recently, there has been considerable interest in numerically modeling the shear bands which result from this constitutive instability [19–21]. The separation of shear flows from homogeneous shear into a banded region of very high shear rate is often accompanied by a plateau of shear stress [21] such as the plateau that we experimentally observed in Fig. 4. The shearing gap here is approximately 3 μm.

Note that the flow curve in Fig. 4 for the cycloaliphatic traction fluid, MCS1218 is non-monotonic. Although this is the only liquid for which we have observed a local maximum in shear stress, the effect was repeatable at a lower pressure. If the shear bands which produce the plateau in our flow curves result from constitutive instability, they may be the result of the "top-jump" described in Ref. [21] when no local maximum shear stress is observed. See the 5P4E in Fig. 4. The band predicted by numerical simulation of constitutive instability operates steadily in a direction parallel to the boundaries and is, therefore, very different from the intermittent inclined bands that we observe in Fig. 3. Additional micrographs of shear band orientation in liquids may be found in Ref. [22].

3. Conclusion

Three models of shear bands in compressed liquids at high shear stress have been discussed. The Mohr–Coulomb failure criterion, which states that slip will occur along a plane where the shear stress has reached a value proportional to the normal stress, provides quantitative predictions of band angles from measurable properties, λ and N_1. We have also shown that NEMD simulation using molecular models can provide one of these properties. A change of character of the governing partial differential equations when piezoviscosity is included offers a mechanism for the propagation of bands in two directions at reasonable stress. Non-monotonic stress-rate behavior is directly observed in one liquid, however, the band orientation is inconsistent with numerical simulations in the literature of bands resulting from constitutive instability.

An important aspect of the traction in lubricated contacts arises when the films are only a few molecular layers thick. In this situation, the shear bands may be restricted to planes parallel to the film. In this case, the observed friction coefficient of the contact should increase from λ to ϕ.

Acknowledgements

S.B. would like to thank the Jacob Wallenberg Foundation and the Timken Company for supporting this work. C.M.C. acknowledges the Donors of the American Chemical Society Petroleum Research Fund for support of this research.

References

[1] Plint MA. Traction in elastohydrodynamic contacts. Proc Inst Mech Eng 1967;182(1):14.
[2] Evans CR, Johnson KL. Rheological properties of elastohydrodynamic lubricants. Proc Inst Mech Eng 1986;200(C5):304.
[3] Bowden PB. In: Haward RN, editor. The physics of glassy polymers. New York: Wiley; 1973, p. 279–339.
[4] Bair S, Qureshi F, Khonsari M. Adiabatic shear localization in a liquid lubricant under pressure. Trans ASME J Tribol 1994;116:705–9.
[5] Bair S, Winer WO, Distin KW. Experimental investigations into shear localization in an operating EHD contact. Leeds–Lyon Symposium on Tribology. Tribology Series, vol. 25. 1992, p. 383–8.
[6] Bair S, Qureshi F, Winer WO. Observations of shear localization in liquid lubricants under pressure. Trans ASME J Tribol 1993;115:507–14.
[7] Ohno N, Shiratake A, Kumamoto S, Kuwano N, Hirano F. Occurrence of shear bands at high pressure. Proceedings of the JAST Tribology Conference. 1997, p. 515–7 [in Japanese].
[8] Bair S, Winer WO. A rheological basis for concentrated contact friction. Proceedings of the 20th Leeds–Lyon Symposium on Tribology. 1994, p. 37–44.
[9] Bair S. Recent advances in high pressure rheology. In: Dowson D, et al., editors. Lubricants and lubrication. Elsevier; 1995, p. 169–87.
[10] Bair S. A new high-pressure, high-shear stress viscometer. Tribol Trans 1993;36(4):721–5.
[11] Bair S. Normal stress difference in liquid lubricants sheared under high pressure. Rheol Acta 1996;35:13–23.
[12] Bair S, McCabe C, Cummings PT. Comparison of nonequilibrium molecular dynamics with experimental measurements in the nonlinear shear-thinning regime. Phys Rev Lett 2002;88(5):058302.
[13] Smit B, Karaborni S, Siepmann JI. Computer-simulations of vapor–liquid phase-equilibria of *N*-alkanes. J Chem Phys 1995;102(5):2126–40.
[14] Mondello M, Grest GS. Molecular-dynamics of linear and branched alkanes. J Chem Phys 1995;103(16):7156–65.
[15] McCabe C, Cui ST, Cummings PT, Gordon PA, Saeger RB. Examining the rheology of 9-octylheptadecane to giga-pascal pressures. J Chem Phys 2001;114(4):1887–91.
[16] Evans DJ, Morriss GP. Statistical mechanics of nonequilibrium liquids. New York: Academic Press; 1990.
[17] Renardy M. Some remarks on the Navier–Stokes equations with a pressure-dependent viscosity. Comm Partial Diff Eqns 1986;11(7):779–93.
[18] Bair S, Khonsari M, Winer WO. High-pressure rheology and limitations of the Reynolds equation. Tribol Int 1998;31(10):582–6.
[19] Cates ME, McLeish TCB, Marrucci G. The rheology of entangled polymers at very high shear rates. Europhys Lett 1993;21(4):454–5.
[20] Spenley NA, Yuan XF, Cates ME. Non-monotonic constitutive laws and the formation of shear banded flows. J Phys II France 1996;6:551–2.
[21] Greco F, Ball RC. Shear band formation in a non-Newtonian fluid model with a constitutive instability. J Non-Newtonian Fluid Mech 1997;69:195–206.
[22] Qureshi F. Kinematics of shear deformation of materials under high pressure and shear stress. Ph.D. Thesis. Georgia Institute of Technology, 1992.